ORIGINAL RESEARCH

Antibacterial Activity of a Novel Biocomposite Chitosan/Graphite Based on Zinc-Grafted Mesoporous Silica Nanoparticles

Donya Jamshidi [ID]
Mohammad Reza Sazegar

Department of Chemistry, Islamic Azad University, Tehran, Iran

Introduction: A novel biocomposite chitosan/graphite based on zinc-grafted mesoporous silica nanoparticles (CGZM-bio) was synthesized and the antibacterial activities of this compound along with that of Zn-MSN nanoparticles were investigated.

Methods: The CGZM-bio biocomposite was synthesized using sol–gel and post-synthesis method under UV radiation. The characterizations of the samples were carried out using FTIR, XRD, SEM, and nitrogen adsorption and desorption. The antibacterial activity was carried out against *Staphylococcus aureus (S. aureus)* and *Escherichia coli (E. coli)* after 18 h at 310 K.

Results: The suspension samples of the Zn-MSN and CGZM-bio (2–100 $\mu g.mL^{-1}$) presented antibacterial activities against *S. aureus* and *E. coli*. The minimum inhibitory concentration (MIC) values against *E. coli* for the Zn-MSN and CGZM-bio samples were 10 and 5 $\mu g.mL^{-1}$, respectively, while the MIC against *S. aureus* for both nanomaterials was 10 $\mu g.mL^{-1}$.

Discussion: The antibacterial activities of these materials are due to the generation of radical oxygen species such as $^{\bullet}OH$, H_2O_2, and O_2^{2-} during the UV radiation via the generation of the electron–hole pairs which in turn damage the bacteria cells. These nanomaterials may be used in biomedical devices as antibacterial agents.

Keywords: Zn-MSN, *Staphylococcus aureus*, *Escherichia coli*, antimicrobial activity, UV radiation, electron–hole pair

Introduction

One of the serious risks for human life with long-lasting disruptive disease is bacterial infections which is the fourth cause of death in the world.[1] The antimicrobial properties of metal nanoparticles (MNPs) and metal oxide nanoparticles (MONPs) are currently studied in various applications of science such as medicine and pharmaceutics.[2,3] The effect of MNPs and MONPs has been credited to their small size and high ratio of surface to volume that make the suitable conditions for interaction of MNPs and MONPs with bacterial membranes.[4,5] Studies found that the bactericidal activity of metal species is related with its valence form[5] and researchers have shown that the higher valence state is the stronger and more active the antimicrobial action.[6,7] The MONPs including silver, titanium, bismuth and zinc oxide nanoparticles have been exhibited antimicrobial effects against Gram-positive and -negative bacteria.[8–11] These materials are able to control bacterial growth.

Silver nanoparticles have long been known as bactericide materials[12–14] which currently exploited in many applications in various fields including medical science,[15] antibacterial water filter[16] and cosmetics.[17] These nanoparticles have been shown the

Correspondence: Mohammad Reza Sazegar
Department of Chemistry, Islamic Azad University, North Tehran Branch, Hakimiyeh, Tehran, Iran
Tel +98-9381199151
Email m_r_sazegar@yahoo.com

most antimicrobial activity among all nanomaterials.[18–20] Recently, composites containing metal atoms dispersed on silica support have been attracted to their high antibacterial activity.[21] The scientists were reported high antibacterial activities for silver-silica and silver-silica-polymer nanocomposites which have used in wound dressings and coating of catheters.[1,22] In addition, several antibacterial activities were reported for ZnO nanoparticles in recent years.[5–7] Moreover, zinc oxide is a low-price semiconductor with simple preparation process, biocompatibility nature and highly active photo-catalyst.[7] These nanomaterials showed notable antimicrobial properties toward a wide range of bacterial types. These nanomaterials have been fixed, impregnated or inserted in other materials such as natural or artificial polymers to enhance their biocidal properties.[23]

Chitosan as a useful natural hydrophilic polymeric matrix has been widely applied recently due to its excellent chemical and biological characteristics.[24,25] Chitosan is prepared from chitin, which is easily extracted from crustacean shells such as fungi, crabs, insects, prawns and other crustaceans.[26] This natural polymer shows non-toxic, biodegradable, biocompatible, bioactive and antimicrobial properties which have made it suitable to apply in medicinal chemistry.[27–29] Chitosan is a weak base due to the presence of an amine group into its structure thus it has solubility in dilute acidic solutions in which this NH_2 group converts into the water-soluble protonated form of NH_3^+[30] Nowadays, chitosan has been widely studied as an antibacterial and anti-fungi material in different forms of solutions, films and composites.[27] Furthermore, the antibacterial property of chitosan changes with notice to fabric samples. This activity of chitosan is due to the interaction between lone pair electrons on the nitrogen atom of amine group with membrane of microbes.[28] Therefore, it is clear that this interaction can be easily carried out between chitosan and microbes because of formation of binds with DNA, glycosaminoglycans and proteins which resulting in an increase in the antibacterial effect.[29] Since these interactions are weak, the antimicrobial property is weak when chitosan applies alone.[28,31–33]

In the last decade, several kinds of chitosan composites have been synthesized in order to use as bactericides.[34,35] Various types of materials have been applied to form composite with chitosan such as carbon nanotube (CNT), graphene oxide and graphite. Among numerous carbon types, graphite possesses especial properties such as large surface area, high porosity and good conductivity.[36] Graphite has recently attracted attention as feasible and cheap filler in composite structures.[37] These outstanding properties may be applicable at the nanoscale, if graphite can be used as thin nanoplatelets.[38] The pure graphite in the form of small thin layers has been studied as substrates to improve the physical and chemical properties of nanomaterials.[39,40] Metal-carbon composites showed antimicrobial activity against *E. coli*.[41] Since the dispersion of carbon substrates such as graphene, CNT and graphite is problematic, the use of these materials as antimicrobial agents is limited. Moreover, the direct contact of carbon materials leads to cell damage, subsequently causing cell death.[42] To improve the antibacterial property of graphene and CNTs, functionalization with metallic nanoparticles has been reported.[42, 43]

Mesoporous silica nanoparticles (MSN) with possessing ordered porous structure, high surface area, large pore size and volume can be acted as hosts for MNPs which resulted in better dispersion of metal sites on the MSN surface.[44,45] The use of MSN as host for metal nanoparticles is an interesting suggestion that increases antimicrobial efficiency.[46,47]

In this study, a biocomposite of chitosan and graphite based on zinc-modified MSN was synthesized and their antibacterial activities were investigated against Gram-positive and Gram-negative microbes like *Staphylococcus aureus (S. aureus)* and *Escherichia coli (E. coli)*. The main goal of this work is to combine the antimicrobial of Zn-MSN and chitosan accompanied with graphite in order to design biocompatible antibacterial biomaterials.

Materials and Methods

Chitosan and graphite were purchased from Kimiya Azma and Black Diamond Companies, Iran, respectively. All other chemicals including cetyltrimethylammonium bromide (CTAB), tetraethylorthosilicate (TEOS), zinc nitrate, and ammonia solution were purchased from Merck Company.

Experimental

Preparation of Zinc Incorporated MSN (Zn-MSN)

Mesoporous silica nanoparticles (MSN) were synthesized by a sol-gel method using cationic surfactant cetyltrimethylammonium bromide (CTAB) as a template and tetraethylorthosilicate (TEOS) as the source of silicon in basic conditions.[44] Cetyltrimethylammonium bromide (CTAB, 1.24 g) was dissolved in double-distilled water (250 g), then ethanol (55 mL) and ammonia solution (10.5 mL, 28%) were added, respectively. After vigorous stirring for approximately 20 min at 298 K, tetraethylorthosilicate (TEOS,

2.7 mL) was added to the mixture. The resulting mixture was stirred for an additional 2 h at 298 K and allowed to rest for 24 h at the same temperature under UV radiation (8 W). The gel molar composition which was applied for the synthesis of the pure MSN was 1.1 TEOS:0.7 CTAB:16 ammonia:91 Ethanol:1053 H_2O. The sample was then collected by centrifugation at 20,000 rpm for 20 min and washed with deionized water and absolute ethanol three times and dried at 383 K for 8 h prior to calcinations. Then, surfactant was removed by calcinations of MSN (1 g) in air at 823 K for 3 h. Zn-incorporated MSN (denoted as Zn-MSN NPs) was prepared by incorporation of zinc into the pure MSN. In this reaction, zinc nitrate (Merck) was used as a precursor of Zinc and the initial molar ratios of Si/Zn was 10. The Zn-MSN samples were synthesized by adding MSN (1 g) into an aqueous solution (50 mL) of zinc nitrate (0.13 g) at 353 K for 12 h followed by centrifugation and drying at 383 K overnight prior to calcination in air at 823 K for 4 h with a heating rate of 1 K min^{-1}.

Synthesis of Chitosan/Graphite/Zn-MSN Biocomposite (CGZM-Bio)

A suspension of Zn-MSN (1 g) in distilled water (100 mL) was sonicated for 30 min. In a separated container, a combination of chitosan (0.2 g), pure graphite (0.1 g), and distilled water (100 mL) were sonicated for 30 min in a separate container. The chitosan-graphite mixture was slowly added to the Zn-MSN suspension and the pH of the mixture was adjusted at 8–9 by micro-addition of NaOH (0.1 M). It was then stirred in a water bath at 343 K for 30 min under UV radiation. The precipitate was washed with distilled water (2 × 40 mL) and dried in a vacuum oven at 333 K.

Antibacterial Test

The antibacterial activities of Zn-MSN nanoparticle and Chitosan/Graphite/Zn-MSN biocomposite were examined against two-pathogenic strains of *Escherichia coli* (*E. coli*), a Gram-negative bacterium, and *Staphylococcus aureus* (*S. aureus*), a Gram-positive bacterium, using agar disc diffusion method. The antibacterial activities were measured by paper disk diffusion assay in terms of minimum inhibitory concentration (MIC) and minimum bactericidal concentration (MBC). In this method, the samples were cultured into a Muller Hinton (MH) and nutrient agar with pH 7.3 on Petri dishes prepared using the *E. coli* and *S. aureus* growth media. The microbes were sprayed evenly on the top of the plates using a sterile glass rod. The microbes were allowed to dry

for 10 min. Then, the test solutions of the samples with different concentrations were dropped into the disk. The culture medium was incubated for 18 h at 310 K. After that, a No. 0.5 Mc-Farland Standard suspension sample, which is equal to $1.5 × 10^8$ Colony-Forming Units per mL (CFU.mL^{-1}), was prepared. The standard dilution micro method was used to perform the antimicrobial effectiveness exams on MH dishes.[48]

Aqueous dispersions of the Zn-MSN nanoparticle and the CGZM-bio samples at several different concentrations were prepared from the initial aqueous dispersion samples. In order to obtain a uniform distribution, the nutrient MH medium was heated to 323 K. In the next step, 10 mL of each sample solution was separately added into Petri dishes including 30 mL of nutrient MH medium. Total volume of 40 mL was kept in each Petri dish and the solution was hardened with MH after 15 min. Then, on each sample, 100 μL of the suspension of microbe was added and spread on the surface of MH medium including the mentioned samples. The Petri dishes were incubated at 310 K for 18 h in a shaking incubator (150 rpm) to grow the microbes. The results were compared to those standard dishes of each of microbes' growth intensity tests in the absence of Zn-MSN NPs or CGZM-biocomposite. The quantitative measurements of the bactericidal activities of Zn-MSN and CGZM-bio were carried out based on the number of CFU growth of bacteria suspension with less concentration (104 CFU) in MH media with different concentrations of Zn-MSN and CGZM-bio samples. In the meantime, all tests were compared to those of the control sample. All experiments were carried out three times for the Zn-MSN nanoparticle and biocomposite under sterile conditions and their results were averaged. The quantitative antibacterial activities were calculated based on decrease ratio (in percent) of the microbes according to eq. 1. as below:

$$R = \frac{n_i - n_f}{n_i} × 100 \qquad (1)$$

where R is the percentage reduction ratio, n_i is the number of bacterial colonies Petri dishes in the control sample test Petri dishes and n_f is the number of bacteria colonies in those Petri dishes after treatment with Zn-MSN and CGZM-bio. In vitro antimicrobial activities of the samples were investigated using disc diffusion method with MH by determining of inhibition zone size in millimeters (mm) according to the standards of the European Committee on Antimicrobial Susceptibility Testing (EUCAST) standards.[49]

The antibacterial effects of Zn-MSN and CGZM-bio were investigated against two pathogenic strains of *E. coli* and *S. aureus*. The initial concentrations of the cultures for the Zn-MSN nanoparticles and CGZM-bio were No. 0.5 Mc-Farland Standard suspension for both microbes, which were determined by using the agar dishes test. Paper plates (disc samples size of 6 mm) coated with the Zn-MSN nanoparticles and CGZM-bio were sterilized by dropping ethanol onto these materials and aging for 10 mins, then placed on the surface of MH which was seeded by 1 mL of microorganism culture. The dishes were inoculated at 310 K for 18 hrs. The inhibition zone size of the disks was measured to determine the antibacterial activity of each sample. An average of three test measurements was used for each sample. In this study, some disks including Amikacin (AN) and Erythromycin (E) standard antibiotics placed on the surface of MH were also applied.

Characterization of the Biocomposite

The crystallinity of catalysts was measured with a Bruker Advance D8 X-ray powder diffractometer with Cu K_α (l = 1.5418 Å) radiation as the diffracted monochromatic beam at 40 kV and 40 mA. Nitrogen physisorption analysis was conducted on a Quantachrome Autosorb-1 at 77 K. Before the measurement, the sample was evacuated at 573 K for

3 h. The bulk Si/Zn molar ratio of 10 was determined by Bruker S4 Explorer X-ray fluorescence spectroscopy (XRF) using Rh as anode target material operated at 20 mA and 50 kV. XRF analysis showed that the Si/Zn ratio of 10 framework was actually 9.3.

Fourier transform infrared (FTIR) measurements were carried out using an Agilent Carry 640 FTIR spectrometer. The morphology and average particle size of the catalyst were estimated from scanning electron microscope (SEM). A scanning electron microscope equipped with an energy dispersion X-ray spectrometer (EDX) was conducted on SEM (JEOL JSM-6701 F) to observe the morphology as well as to obtain the elemental analysis of the catalyst. Before observation by SEM-EDX, the sample was coated by Pt using a sputtering instrument.

Results and Discussion
Catalyst Characterization

The pure MSN was synthesized through the sol–gel method and the Zn-MSN sample was prepared by post-synthesis technique, respectively. XRD patterns of the MSN, Zn-MSN and CGZM-bio samples with Si/Zn molar ratio of 10 are given in Figure 1. The pure MSN exhibited four diffraction peaks included an intense peak of 100 and three small peaks of 110, 200 and 210 at low angle degree
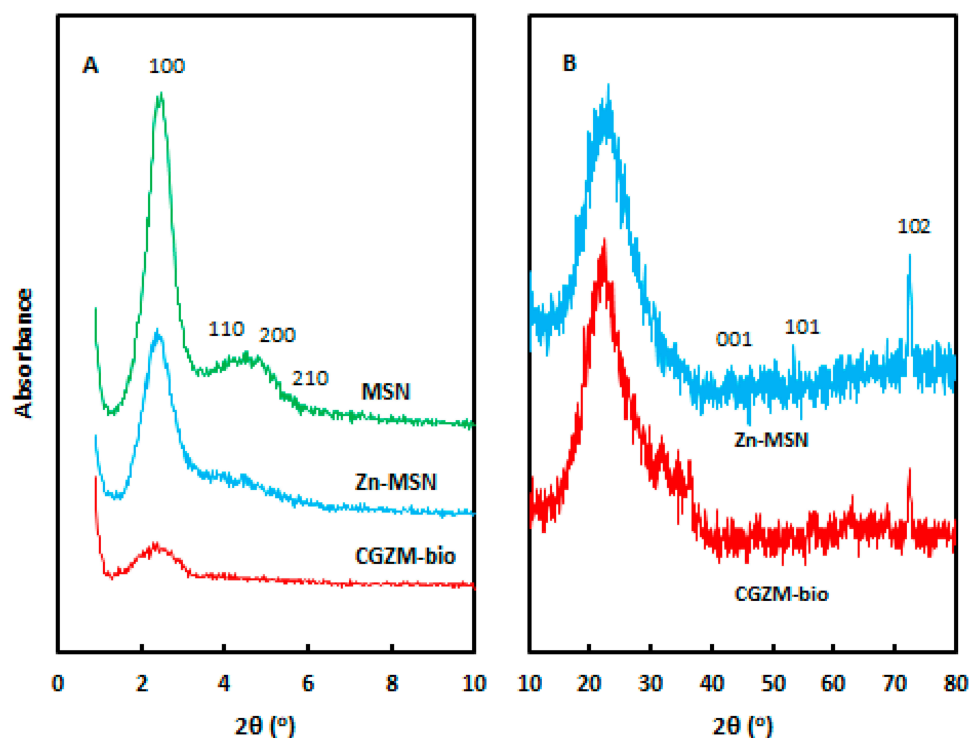

Figure 1 XRD patterns: (**A**) low degree at 0-10° for MSN, Zn-MSN, and CGZM-bio; (**B**) high degree at 10-80° for Zn-MSN, and CGZM-bio.

at 2θ of 2.2–5.6°. All these diffraction peaks showed the presence of 2D hexagonal (p6mm) structure with a d_{100}-spacing of approximately 3.7 nm. Incorporation of zinc atoms into MSN decreased the intense peak of 100 due to a decrease in the order of mesoporous structures.[50] Introducing of chitosan and graphite into the Zn-MSN nanoparticles drastically reduced this intense peak and consequently have completely altered the mesoporous structure to a less order structure. The small shift in the peak position from 2.35° in MSN to 2.20° in Zn-MSN could be explained by the substitution of Si specious with zinc atoms with larger atomic radius which led to a decrease in the interplanar spacing of MSN (Figure 1A). The high angle XRD patterns at 10-80° for the MSN, Zn-MSN-10 and CGZM-bio samples are shown in Figure 1B. The X-ray microanalysis of these materials exhibited the presence of zinc atoms in their structures. The peaks corresponded to the diffractions of 001, 101 and 102 planes indicated the presence of ZnO phase in these nanostructures.[51]

The diffraction patterns also revealed that the Zn-MSN samples had a good crystallinity. Intercalation of zinc ions within the interlayer spacing of MSN resulted in an increase in the basal spacing due to the replacement of exchangeable interlayer atoms. The existence of chitosan and graphite into the MSN framework was also reflected by the presence of the amorphous structure, as shown in the diffraction patterns of Figure 2B.

Table 1 shows the physical properties of the MSN, Zn-MSN, and CGZM-bio samples. The surface area was decreased from 892 m^2g^{-1} in MSN to 475 m^2g^{-1} in Zn-MSN, which was due to the loading of Zn species into the pure MSN. It consequently decreased the pore volume and pore size of Zn-MSN. This result probably due to the plugging of some pores by zinc atoms that caused a change of the pore size from 3.41 nm in MSN to 3.36 nm in ZN-MSN and also altered the pore volume from 0.72 cm^3g^{-1} in MSN to 0.43 cm^3g^{-1} in Zn-MSN.[45]

An introduction of chitosan and graphite to the mesoporous Zn-MSN nanoparticles completely changed the structure of microporous material. It is believed that chitosan and graphite thoroughly plugged most of pores and drastically reduced the pore surface area of CGZM-bio to 13 m^2g^{-1} while increased the pore size to 36.6 nm. These results clearly showed that this biocomposite possesses a dense structure with a wide pore and the SEM images confirmed its morphology (Figure 3).

Figure 2A and B show nitrogen sorption isotherms and the corresponding pore size distribution of the MSN, Zn-MSN NPs, CGZM-bio samples which were calculated by NLDFT method. The nitrogen sorption isotherm patterns of these nanomaterials showed type IV isotherms for the pure and Zn-modified MSN which are an indication of the presence of mesoporous nanomaterials with cylindrical pores, and showed type III Isotherm for CGZM-bio which is
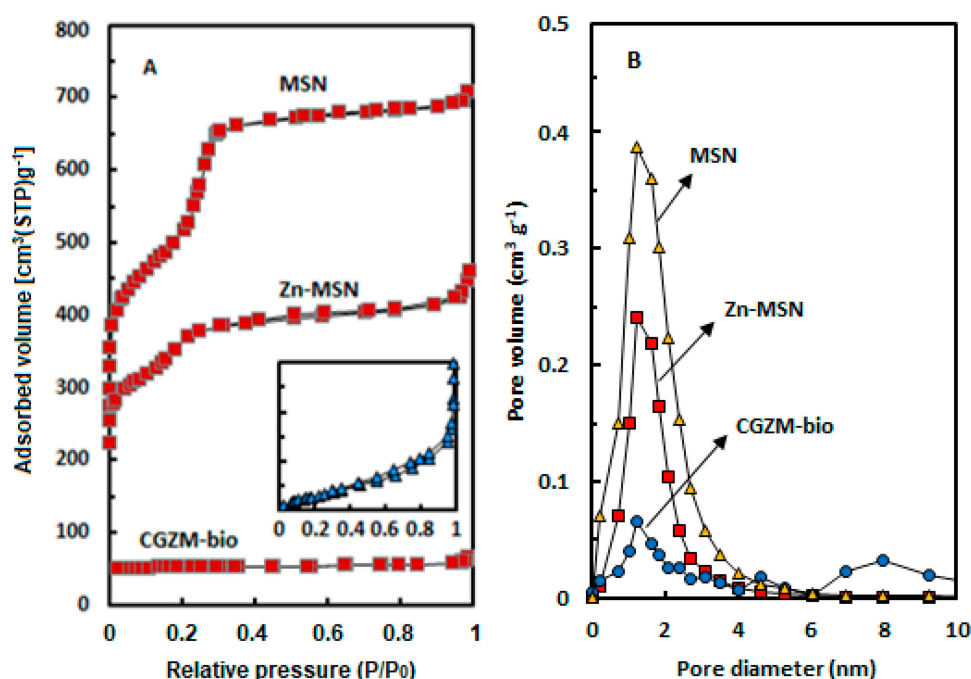

Figure 2 (**A**) Nitrogen sorption isotherms and (**B**) pore size distribution for the MSN, Zn-MSN NPs, and CGZM-bio samples.

Table 1 Physical Characteristics of the MSN, Zn-MSN NPs and CGZM-Bio Samples

Sample	S (m²/g)	Vp (cm³/g)	W (nm)
MSN	892	0.72	3.41
Zn-MSN NPs	475	0.43	3.36
CGZM-bio	13	0.10	36.6

Abbreviations: S, BET surface area (m²/g) obtained from N_2 adsorption; V_p, total pore volume (cm³/g); W, pore size (nm) obtained from BJH method.

attributed to the microporous structure (Figure 2A). The high resolution of CGZM-bio sample was observed in the square which clearly exhibited the microporous construction with extra-framework structure. The isotherms of the MSN and Zn-MSN show the inflection characteristic of capillary condensation at a relative pressure (P/P₀) of around 0.1–0.3 which exhibits the existence of porous structures with small and uniform mesopore structures.[52] A small increase at high relative pressure of around 0.9–1.0 in the Zn-MSN indicated the presence of the external-framework porosity which is a clear evidence of less ordered mesoporous structure due to

the zinc atoms loaded into the pure mesoporous silica materials. For CGZM-bio composite, a slow increase was observed from 0 to 0.9 relative pressure that attributes to the microporous structure while a sharp increase at P/P₀ around 0.9–1.0 indicates the presence of an extra-framework structure into the biocomposite. Figure 2B exhibits the pore size distribution of MSN, Zn-MSN NPs and CGZM-bio. The results showed that the incorporation of chitosan, graphite and zinc atoms almost plugged the biocomposite pores which led to the formation of several pore diameters into the composite framework.

The morphologies of MSN, Zn-MSN and CGZM-bio were observed using SEM and TEM images which are shown in Figure 3. The results showed uniform spherical particles with particle sizes of 70–130 nm for MSN and Zn-MSN, along with its EDX elemental. Changes on the surface structure of CGZM-bio were also obvious from its SEM image as presented in Figure 3C. A big spherical layer-like feature with sizes of more than 200 nm was also observed for CGZM-bio. The rough surface of the biocomposite revealed
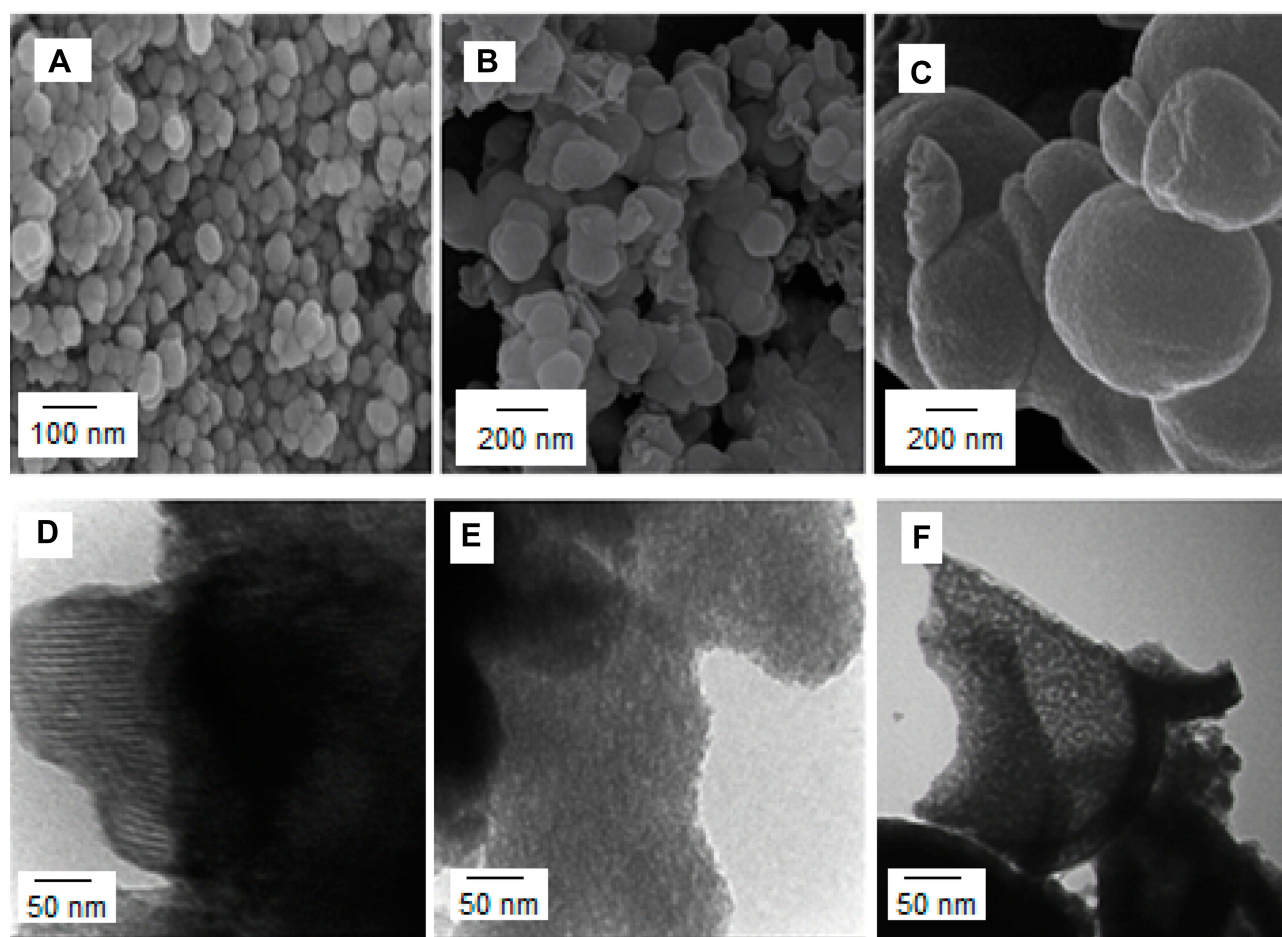
Figure 3 SEM and TEM images of the (**A, D**) MSN, (**B, E**) Zn-MSN NPs, (**C, F**) CGZM-bio samples.

that the Zn-MSN nanoparticles have been assembled on chitosan and graphite layers led to the formation of big spherical-layered structure. The TEM images of MSN, Zn-MSN and CGZM-bio are shown in Figure 3(D–F). The mesoporous framework of the MSN was confirmed by TEM (Figure 3D) which exhibited regular and parallel pore structure.[53] The TEM image of the Zn-MSN sample (Figure 3E) shows material grains with a regular array of mesoporous structure. Zn atoms are well dispersed in the silica matrices. The TEM of CGZM-bio sample (Figure 3F) shows the spherical monolithic grains in this sample. The framework silica mesopores are wormhole-like throughout the grain. No clear long-range order in the pore structure was detected.[54]
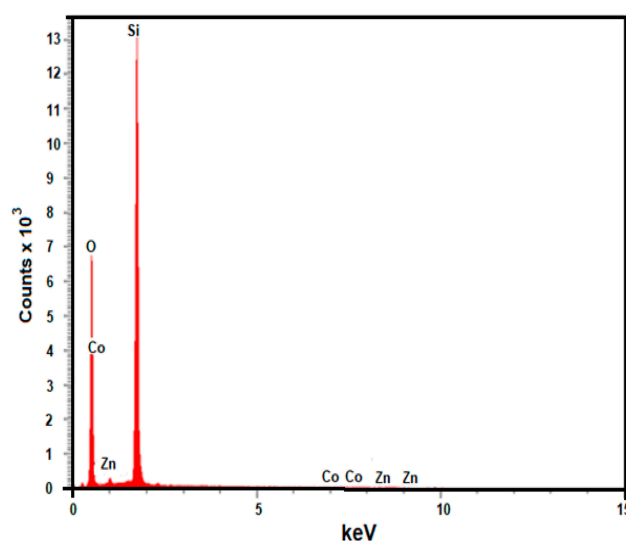

Figure 4 Energy-dispersive X-ray spectroscopy of the Zn-MSN sample.

The EDX analysis, shown in Figure 4, indicated to the presence of silicon, zinc and oxygen in the Zn-MSN nanomaterials.

Figure 5 shows the FTIR spectroscopy of the MSN, Zn-MSN NPs and CGZM-bio samples. The silanol (Si-OH) groups of MSN and zinc-modified MSNs were observed as the broad bands at the range of 3100–3700 cm^{-1}. These wide peaks assigned to the non-acidic silanol groups which are located on the external surface of the mesoporous structure.[55] A small sharp band at the region of 3405 cm^{-1} indicated to the presence of amine group within the biocomposite material. In addition, two sharp bands at 2923 and 2852 cm^{-1} are clear evidence of the C-H stretching due to the presence of chitosan and graphite species in the biocomposite structure. The peaks around 1636 cm^{-1} corresponds to amide structure of chitosan.[56] Grafting of zinc into the MSN structure formed a sharper band at 3445 cm^{-1} due to the reaction of silanol groups with Zn atoms and formation of the Si-O-Zn band.[45] There are no remarkable differences in the d_{100}-spacing or pore diameters and also in the band intensities in this region (3445 cm^{-1}) for MSN and Zn-MSN which show that their primary particle sizes are comparable.[57] Two vibration peaks of FTIR spectrum located at the regions of 465 and 1070 cm^{-1} are associated with the Si-O stretching frequency in the mesoporous silica materials, in which these peaks correspond to the bonds O–Si–O and Si–O–Si, respectively. Whereas the absorption peak at 796 cm^{-1} assigned to the Si-O-Si bending vibration in the sample structures.[58]

The proposed structure of CGZM-bio was shown in Scheme 1. It is suggested that the Zn-MSN is linked to
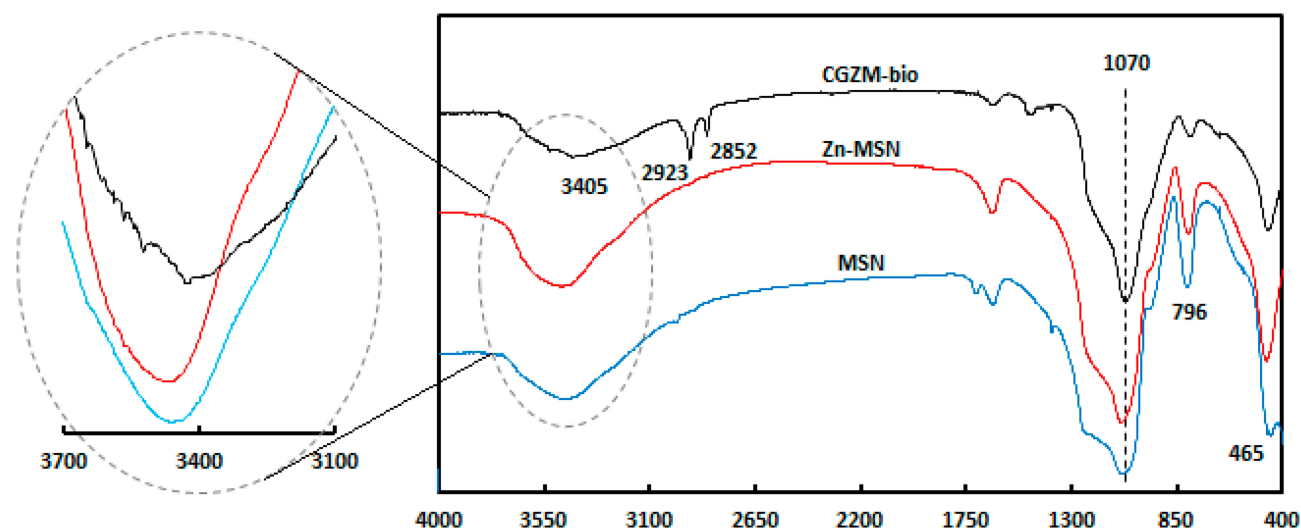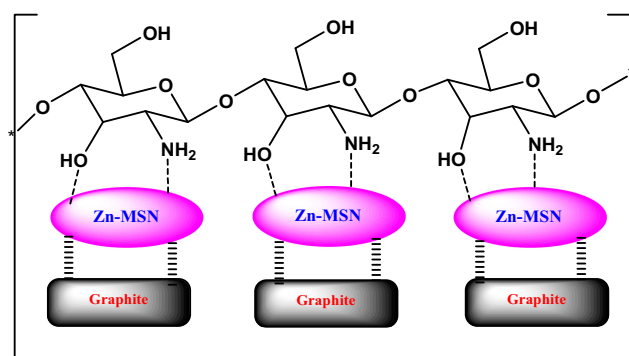

Figure 5 FTIR spectra of MSN, Zn-MSN NPs, and CGZM-bio in the region of 400–4000 cm^{-1}.

Scheme 1 Proposed structure for CGZM-biocomposite.

chitosan through electrostatic bands between amine groups of chitosan and Zn atoms of Zn-MSN nanoparticles while there are other bands between graphite molecules with Si-O-Si bands of Zn-grafted MSN nanomaterials.

Evaluation of Antibacterial Activity

The antibacterial activity of the Zn-MSN nanoparticles and CGZM-bio suspensions against *E. coli* and *S. aureus* was studied in aqueous MH agar by disk diffusion and their MIC and MBC were measured. The MBC is the lowest concentration (μg mL^{-1}) at which a material will kill more than 99% of the existing microbes. The MIC is the concentration at which the solution becomes turbid. A lower MIC corresponds to higher antimicrobial efficiency.[59] In terms of MIC, we found an inverse relationship between the particle size and activity. For the qualitative valuation of antimicrobial activity of the stated materials, MH disk including the noticed nanoparticles and biocomposite with different concentrations were insemi-nated with bacterial suspension 1.5×10^8 CFU. The results showed that the bacteria growth on MH plates was observed after 18 h at different concentrations of the Zn-MSN nanopar-ticles and CGZM-bio ranging from 5, 10 and 100 μg mL^{-1}. The control sample occurred with 0 μg mL^{-1} Zn-MSN and biocomposite in 1% acetic acid solution and the microbes were completely grown after 18 h at 310 K. The results showed the MIC values of Zn-MSN and CGZM-bio against *E. coli* were 10 μg.mL^{-1} and 5 μg.mL^{-1}, respectively, and against *S. aureus* were 10 μg.mL^{-1} for both nanomaterials. The MIC value for control sample was measured about 900 μg.mL^{-1} for *E. coli*[60] and 1550 μg.mL^{-1} for *S. aureus*.[61] The results exhibited that there was no bacteria growth at the MIC values and above, therefore these concentrations are the effective inhibition in both the bacterial growth.

According to the published results, the antibacterial activity of chitosan and graphite was weak when used

alone.[32,62] The mechanism of the biocomposite is the inhibition of bacterial growth, may be through the forma-tion of cationic section on the zinc atom and amine group, and interact with the anionic part on the microbial cell surface, and may destroy bacterial growth by damaging the exchanges with the medium.[61] The inhabitation mechanism of bacterial growth for the Zn-MSN nanopar-ticles is probably via the interaction between zinc sites with the bacterial membrane.

Recently, N. Padmavathy and R. Vijayaraghavan (2008) have stated the qualitatively antimicrobial effect of ZnO nanoparticle suspensions with sizes of 12 nm and 45 nm toward *E. coli* in aqueous Luria Bertani (LB) broth by disk diffusion. They have reported the quantitative measurement of 80 μg.mL^{-1} against *E. coli* at 310 K.[61,63] Sharifian-Esfahni et al (2017) were synthesized the chitosan-modified iron oxide (SPIO/CTS) nanocompo-site to improve the antibacterial activities against *E. coli* and *S. aureus*. The results showed that the SPIO/CTS nanocomposite exhibited MIC values of 45 μg.mL^{-1} for *E. coli*.[64] In another study, Hu et al (2017) prepared a nanocomposite based on using zinc oxide with silver nanoencapsulated in polyvinylpyrrolidone and polycapro-lactone (PVP/PCL) nanofibers to increase the antibacterial effectiveness against *S. aureus* and *E. coli* under MH broth medium. The results indicated that the suspension of this nanocomposite able to inhibit bacterial growth against these two microbes.[65] This increased antibacterial strength is probably due to the enhanced stability of the biomaterial in aqueous medium since that the composite of chitosan/graphite protected the Zn-MSN nanoparticles from aggre-gation. The significant antibacterial activity over *E. coli* under low concentration of the biocomposite can be used as an ideal nanomaterial with long-lasting effect in green industrials.
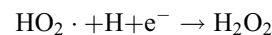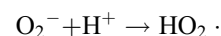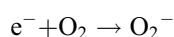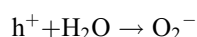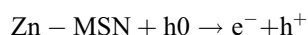
Comparison of inhibition zone diameter (IZD) test for Amikacin (AN) (30 μg.disk^{-1}) and Erythromycin (E) (15 μg.disk^{-1}) as two standard antibiotics, the Zn-MSN NPs and CGZM-bio that have content of 5, 10 and 100 μg. mL^{-1} on MH plate against *E. coli* and *S. aureus* bacterium. The IZD surrounding both samples were observed with the average diameter of 21±1 mm against *E. coli* for both samples of Zn-MSN NPs and CGZM-bio with the concen-trations of 10 μg.disk^{-1}. The results were 22±1 mm and 24±1 mm against *S. aureus* for Zn-MSN NPs and CGZM-bio, respectively, with the concentrations of 10 μg.disk^{-1}.

The results of the antimicrobial activities of the sam-ples indicated that the organic layer of chitosan/graphite

related to the biocomposite probably is responsible for more strength of the activity of the biocomposite due to the better dispersion of the Zn-MSN NPs on the surface of the Chitosan/graphite part. Any IZD were not observed around the control samples against both bacteria using this disk. Table 2 shows the obtained results for two samples of the Zn-MSN NPs and CGZM-bio against both bacteria of *E. coli* and *S. aureus*.

Several factors can be caused that the Zn-MSN NPs and CGZM-bio to be bactericidal. The mechanism that antibacterial agents and antibiotics act through the oxidative stress generated by reactive oxygen species (ROS).[66] Park and his colleagues have been explained that the generation of ROS was the reason for the antibacterial activity of metal.[67]

In this study, zinc oxide is the source of the ROS formation which leading to the *S. aureus* and *E. coli* inhibition. The mechanism of the activity of Zn-MSN NPs and biocomposite is based on the generation of the oxygen species by these materials which cause damage to the microorganisms.[68] The high reactive species such as $^{\bullet}OH$, H_2O_2 and O_2^{2-} were formed. Since Zn-MSN part can be activated by UV radiation through the generation of electron-hole pairs (e^-h^+) which dissociated H_2O molecules into OH^- and H^+. Superoxide radical anions ($^{\bullet}O_2^-$) were formed after dissolving oxygen molecules, which reacted with H^+ to generate $HO_2^{\bullet}$ radicals, resulting generate hydrogen peroxide anions of HO_2^- due to collision with electrons. These anions react with H^+ and produce H_2O_2 molecules that penetrate the bacterial membrane and kill the microbes.[69]

$$Zn - MSN + h0 \rightarrow e^- + h^+$$

$$h^+ + H_2O \rightarrow O_2^-$$

$$e^- + O_2 \rightarrow O_2^-$$

$$O_2^- + H^+ \rightarrow HO_2 \cdot$$

$$HO_2 \cdot + H + e^- \rightarrow H_2O_2$$

The superoxide and hydroxyl radical possesses negative charges which cannot penetrate into the membranes of bacteria and contact only with the outer surface of the microbes. However, hydrogen peroxide can penetrate into the bacterial membranes.[70] An explanation of the antimicrobial effect of Zn-MSN NPs probably based on the rough surface of this nanoparticle due to their surface defects.[71] This surface roughness provides a mechanical damage of the membrane of *E. coli*.

In this study, the minimum inhibitor concentration (MIC) range of the Zn-MSN and CGZM-bio nanomaterials was between 2 and 100 (μg/mL) for both *E.coli* and *S. aureus* bacteria. According to the obtained results, the concentrations of 5 and 10 μg/mL for CGZM-bio and Zn-MSN showed the minimum inhibitor against *E. coli* microbe, while the minimum inhibitor concentration for both nanomaterials against *S. aureus* was 10 μg/mL. The MIC and MBC results of both samples of Zn-MSN and CGZM-bio against *E.coli* and *S. aureus* bacteria were approximately equal.

Thus, the sample suspensions in lower concentrations than 10 and 5 μg.mL^{-1} for Zn-MSN and CGZM-bio, respectively, show less antibacterial activity against *E. coli* and *S. aureus* bacteria, respectively. This may be due to the presence of the low zinc content to generate the mentioned radical species. The growth of *E. coli* bacterium at lower concentration of 5 μg.mL^{-1} around the disk including biocomposite and the growth of *S. aureus* at lower concentration of 10 μg.mL^{-1} around the disk of Zn-MSN can be evidenced to confirm the direct relation between bacterial activity and Zn concentration. On the other hand, the zinc is not toxic at these low concentrations, since this metal is an essential cofactor in many cellular processes. Therefore, the bacterial colony

Table 2 IZD, MIC and MBC of the Zn-MSN NPs and CGZM-Bio Samples

Bacteria	IZD Control Sample (mm)	MIC Control Sample (μg. mL^{-1})	Standard Antibiotic AN (30 μg.disk^{-1})	Standard Antibiotic E (15 μg. disk^{-1})	IZD		MIC		MBC	
					Zn-MSN (mm)	CGZM-Bio (mm)	Zn-MSN (μg. mL^{-1})	CGZM-Bio (μg. mL^{-1})	Zn-MSN (μg. mL^{-1})	CGZM-Bio (μg. mL^{-1})
E. coli	0	900	20±1	20 ±1	21±1	21±1	10	5	10	5
S. aureus	0	1550	13±1	21±1	22±1	24±1	10	10	10	10

Abbreviations: CGZM-bio, biocomposite chitosan/graphite based on zinc-grafted mesoporous silica nanoparticles; Zn-MSN, Zinc-grafted mesoporous silica nanoparticles; EUCAST, European Committee on Antimicrobial Susceptibility Testing; *E. coli, Escherichia coli*; *S. aureus, Staphylococcus aureus*; FTIR, Fourier Transfer Infra-Red; SEM, S Emission Microscopy, TEM, Transmission Emission Microscopy; BET, Burette Emmer Teller; XRD, X-ray diffraction.
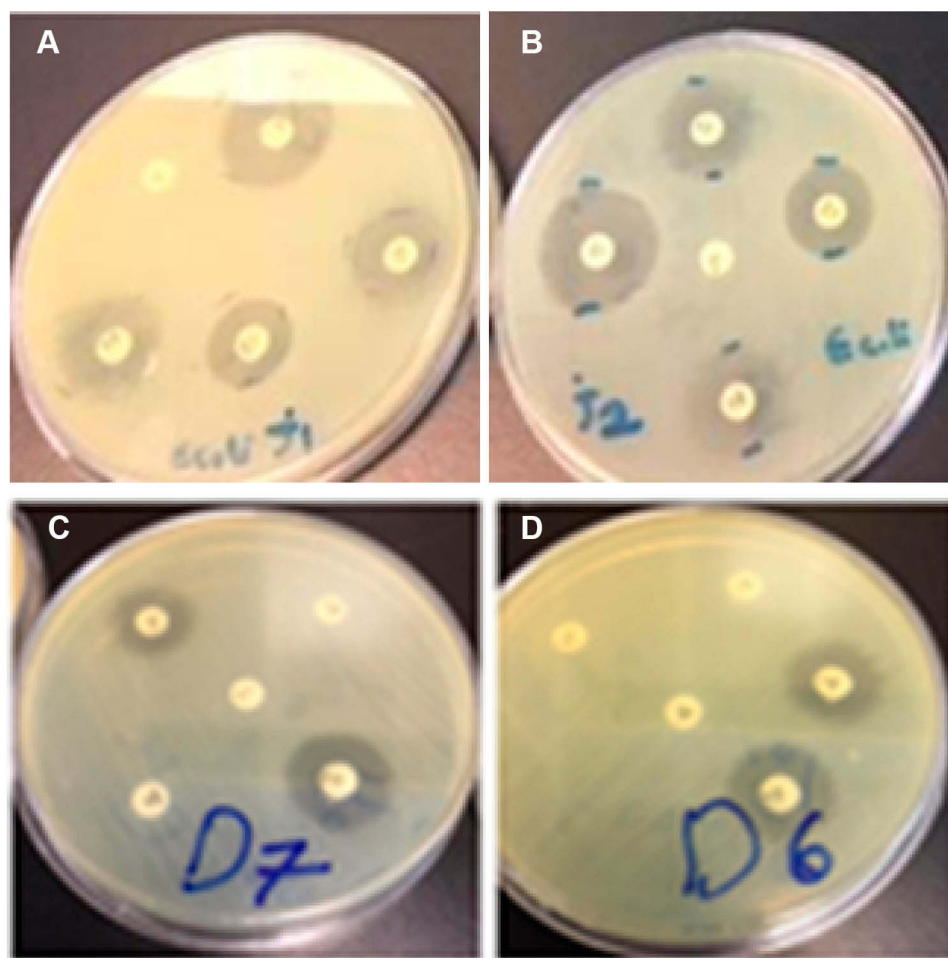
Figure 6 Images of the antibacterial tests against *E. coli* for (**A**) 5 μg/mL of CGZM-bio, (**B**) 10 μg/mL Zn-MSN, and the antibacterial tests against *S. aureus* for 10 μg/mL (**C**) CGZM-bio, and (**D**) Zn-MSN.

generation in the amounts less than MIC, demonstrating that Zn species are the supplement promoting the metabolic performance of bacteria at the low concentrations.

Figure 6 shows the photography of the antibacterial activities against *E. coli* and *S. aureus* bacteria for the CGZM-bio, Zn-MSN samples.

Conclusion

The novel Zn-MSN NPs and CGZM-bio nanomaterials were prepared using UV radiation and their antimicrobial activities were investigated. The biocomposite nanomaterial was synthesized based on an inorganic part (Zn-MSN) combined with chitosan/graphite as the organic part. The colloidal solutions of the Zn-MSN nanoparticles and CGZM-bio ranging from 5, 10, and 100 μg mL^{-1} exhibited the antibacterial activity against gram-positive (*S. aureus*) and gram-negative (*E. coli*) microbes on MH dishes after 18 h at 310 K at all three concentrations. The MIC values of Zn-MSN NPs and

CGZM-bio against *E. coli* were 10 μg.mL^{-1} and 5 μg.mL^{-1}, respectively, and against *S. aureus* were 10 μg.mL^{-1} for both nanomaterials. The MBC values of Zn-MSN and CGZM-bio against *E. coli* and *S. aureus* were almost the same as those MIC values.

The inhibition zone diameter (IZD) surrounding the samples was observed with the average diameter of 21±1 mm against *E. coli* for both samples of Zn-MSN NPs and CGZM-bio with the concentrations of 10 μg. disk^{-1}. Similar observation against S. *aureus* resulted in 22±1 mm and 24±1 mm against *S. aureus* for Zn-MSN NPs and CGZM-bio, respectively, with the concentrations of 10 μg.disk^{-1}. The antibacterial characteristic of the Zn-MSN NPs and biocomposite is based on the generation of oxygen species such as $^{\bullet}OH$, H_2O_2 and O_2^{2-} by these materials which cause damage of the microorganisms. Therefore, these nanomaterials may be suitable for antibacterial applications in biomedical devices.

Acknowledgments

Disclosure

The authors report no conflicts of interest in this work.

References

1. Sethi S, Murphy TF. Bacterial infection in chronic obstructive pulmonary disease in 2000: a state-of-the-art review. *Clin Microbiol Rev.* 2001;14:336–363. doi:10.1128/CMR.14.2.336-363.2001

2. Akhavan O, Azimirad R, Moshfegh AZ. Low temperature self-agglomeration of metallic Ag nanoparticles of on silica sol–gel thin films. *J Phys D Appl Phys.* 2008;41:195305. doi:10.1088/0022-3727/41/19/195305

3. Dorjnamjin D, Ariunaa M, Shim YK. Synthesis of silver nanoparticles using hydroxyl functionalized ionic liquids and their antimicrobial activity. *Int J Mol Sci.* 2008;9:807–820. doi:10.3390/ijms9050807

4. Morones JR, Elechiguerra JL, Camacho A, et al. The bactericidal effect of silver nanoparticles. *Nanotechnology.* 2005;16:2346–2353. doi:10.1088/0957-4484/16/10/059

5. Wu F-C, Tseng R-L, Juang R-S. A review and experimental verification of using chitosan and its derivatives as adsorbents for selected heavy metals. *J Environ Manage.* 2010;91:798–806. doi:10.1016/j.jenvman.2009.10.018

6. Khan SB, Alamry KA, Bifari EN, et al. Assessment of antibacterial cellulose nanocomposites for water permeability and salt rejection. *J Ind Chem.* 2015;24:266–275.

7. Selvin R, Hsu HL, Arul NS, et al. Comparison of photo-catalytic efficiency of various metal oxide photo-catalysts for the degradation of methyl orange. *Sci Adv Mater.* 2010;2:58–63. doi:10.1166/sam.2010.1072

8. Hong RY, Li JH, Chen DLL, et al. Synthesis, surface modification and photocatalytic property of ZnO nanoparticles. *Powder Technol.* 2009;189:426–432. doi:10.1016/j.powtec.2008.07.004

9. Ruparelia JP, Chatterjee AK, Duttagupta SP, et al. Strain specificity in antimicrobial activity of silver and copper nanoparticles. *Acta Biomater.* 2008;4:707–716. doi:10.1016/j.actbio.2007.11.006

10. Yadollahi M, Gholamali I, Namazi H, et al. Synthesis and characterization of antibacterial cellulose/ZnO carboxymethyl nanocomposite hydrogels. *Int J Biol Macromol.* 2015;74:136–141. doi:10.1016/j.ijbiomac.2014.11.032

11. Lu Z, Gao J, He Q, et al. Enhanced Antibacterial and wound chitosan-Ag/ZnO healing activities of microporous composite dressing. *Carbohydr Polym.* 2017;156:460–469. doi:10.1016/j.carbpol.2016.09.051

12. Fortuny A, Bengoa C, Font J, et al. Bimetallic catalysts for continuous catalytic wet air oxidation of phenol. *J Hazard Mater.* 1999;64:181. doi:10.1016/S0304-3894(98)00245-3

13. Cho KH, Park JE, Osaka T, et al. The study of antimicrobial activity and preservative effects of nanosilver ingredient. *Electrochim Acta.* 2005;51:956–960. doi:10.1016/j.electacta.2005.04.071

14. Rai M, Yadav A, Gade A. Silver nanoparticles as a new generation of antimicrobials. *Biotechnol Adv.* 2009;27:76–83. doi:10.1016/j.biotechadv.2008.09.002

15. Xu K, Wang JX, Kang XL, et al. Fabrication of antibacterial monodispersed Ag–SiO2 core–shell nanoparticles with high concentration. *Mater Lett.* 2009;63:31–33. doi:10.1016/j.matlet.2008.08.039

16. Kokura S, Handa O, Takagi T, et al. Silver nanoparticles as a safe preservative for use in cosmetics. *Nanomed: Nanotechnol Biol Med.* 2010;6:570–574. doi:10.1016/j.nano.2009.12.002

17. Jain J, Arora S, Rajwade JM, et al. Silver nanoparticles in therapeutics: development of an antimicrobial gel formulation for topical use. *Mol Pharm.* 2009;6:1388–1401. doi:10.1021/mp900056g

18. Gaballah ST, El-Nazer HA, Abdel-Monem RA, El-Liethy MA, Hemdan BA, Rabie ST. Synthesis of novel chitosan-PVC conjugates encompassing Ag nanoparticles as antibacterial polymers for biomedical applications. *Int. J. Biol. Macromol.* 2019;121:707–717. doi:10.1016/j.ijbiomac.2018.10.085

19. Wu Y, Yang Y, Zhang Z, Wang Z, Zhao Y, Sun L. Fabrication of cotton fabrics with durable antibacterial activities finishing by Ag nanoparticles. *Text Res J.* 2019;89:867–880. doi:10.1177/0040517518758002

20. Phuruangrat A, Siri S, Wadbua P, Thongtem S, Thongtem T. Microwave-assisted synthesis, photocatalysis and antibacterial activity of Ag nanoparticles supported on ZnO flowers. *J Phys Chem Solids.* 2019;126:170–177. doi:10.1016/j.jpcs.2018.11.007

21. Roe D, Karandikar B, Bonn-Savage N, et al. Antimicrobial surface functionalization of plastic catheters by silver nanoparticles. *J Antimicrob Chemother.* 2008;61:869–876. doi:10.1093/jac/dkn034

22. Kim YH, Lee DK, Cha HG, et al. Synthesis and characterization of antibacterial Ag–SiO2 nanocomposite. *J Phys Chem C.* 2007;111:3629–3635. doi:10.1021/jp068302w

23. Adams AP, Santschi EM, Mellencamp MA. Antibacterial properties of a silver chloride-coated nylon wound dressing. *Vet Surg.* 1999;28:219–225. doi:10.1053/jvet.1999.0219

24. Chen G, Haase H, Mahltig B. Chitosan-modified silica sol applications for the treatment of textile fabrics: a view on hydrophilic, antistatic and antimicrobial properties. *J Sol-Gel Sci Technol.* 2019;91:461–470. doi:10.1007/s10971-019-05046-8

25. Zhu T, Jiang J, Zhao J, Chen S, Yan X. Regulating preparation of functional alginate-chitosan three-dimensional scaffold for skin tissue engineering. *Int J Nanomedicine.* 2019;14:8891–8903. doi:10.2147/IJN.S210329

26. Ibrahim NA, Eid BM, Khalil HM. Cellulosic/wool pigment prints with remarkable antibacterial functionalities. *Carbohydr Polym.* 2015;115:559–567. doi:10.1016/j.carbpol.2014.09.013

27. Jayakumar R, Nagahama H, Furuike T, et al. Synthesis of phosphorylated chitosan by novel method and its characterization. *Int J Biol Macromol.* 2008;42:335–339. doi:10.1016/j.ijbiomac.2007.12.011

28. Zhao L, Mitomo H, Zhai M, et al. Synthesis of antibacterial PVA/CM-chitosan blend hydrogels with electron beam irradiation. *Carbohydr Polym.* 2003;53:439. doi:10.1016/S0144-8617(03)00103-6

29. Kumar M, Muzzarelli RAA, Muzzarelli C, et al. Chitosan chemistry and pharmaceutical perspectives. *Chem Rev.* 2004;104:6017. doi:10.1021/cr030441b

30. Kim EH, Ahn Y, Lee HS. Biomedical applications of superparamagnetic iron oxide nanoparticles encapsulated within chitosan. *J Alloys Compd.* 2007;434:633–639. doi:10.1016/j.jallcom.2006.08.311

31. Chen CS, Liau WY, Tsai GJ. Antibacterial effects of N-sulfonated and N-sulfobenzoyl chitosan and application to oyster preservation. *J Food Prot.* 1998;61:1124. doi:10.4315/0362-028X-61.9.1124

32. Juntarapun K, Satirapipathku C, The 4th RMUTP International Conference: Textiles & Fashion Bangkok Thailand Section II 2012: 1.

33. Jovancic D, Jocic D, Molina R, et al. Shrinkage properties of peroxide-enzyme biopolymer treated wool. *Text Res J.* 2001;71:948. doi:10.1177/004051750107101103

34. Vimala K, Mohan YM, Varaprasad K, et al. Fabrication of curcumin encapsulated chitosan-PVA silver nanocomposite films for improved antimicrobial activity. *Biom J Nanobio.* 2011;2:55.

35. Boddu VM, Abburi K, Talbott JL, et al. Removal of arsenic (III) and arsenic (V) from aqueous medium using chitosan-coated biosorbent. *Water Res.* 2008;42:633–642. doi:10.1016/j.watres.2007.08.014

36. Liu H, Zhang L, Yan M, Yu J. Carbon nanostructures in biology and medicine. *J Mater Chem B.* 2017;5:6437–6450. doi:10.1039/C7TB00891K

37. Liu Q, Liu Y, Tang S, et al. Effects of morphological characteristics of graphite fillers on the thermal conductivity of the graphite/copper composites fabricated by vacuum hot pressing sintering. *Vacuum*. 2019;167:199–206. doi:10.1016/j.vacuum.2019.06.011

38. Bhatnagar A, Sillanpää M. Applications of chitin- and chitosan-derivatives for the detoxification of water and wastewater-A short review. *Adv Colloid Interface Sci*. 2009;152:26–38. doi:10.1016/j.cis.2009.09.003

39. Stankovich S, Dikin DA, Dommett GHB, et al. Graphene-based composite materials. *Nature*. 2006;442:282–286. doi:10.1038/nature04969

40. Fan L, Luo C, Li X, et al. Fabrication of novel magnetic chitosan grafted with graphene oxide to enhance adsorption properties for methyl blue. *J Hazard Mater*. 2012;215-216:272–279. doi:10.1016/j.jhazmat.2012.02.068

41. Fan L, Luo C, Sun M, et al. Preparation of novel magnetic chitosan/graphene oxide composite as effective adsorbents toward methylene blue. *Bioresour Technol*. 2012;114:703–706. doi:10.1016/j.biortech.2012.02.067

42. Akhavan O, Abdolahad M, Abdi Y, et al. Silver nanoparticles within vertically aligned multi-wall carbon nanotubes with open tips for antibacterial purposes. *JMCh*. 2011;21:387–393.

43. Amiri A, Zardini HZ, Shanbedi M, et al. Efficient method for functionalization of carbon nanotubes by lysine and improved antimicrobial activity and water-dispersion. *Matl*. 2012;72:153–156.

44. Sazegar MR, Mahmoudian S, Mahmoudi A, et al. Catalyzed Claisen–Schmidt reaction by protonated aluminate mesoporous silica nanomaterial focused on the (E)-chalcone synthesis as a biologically active compound. *RSC Adv*. 2016;6:11023–11031. doi:10.1039/C5RA23435B

45. Sazegar MR, Dadvand A, Mahmoudi A. Novel protonated Fe-containing mesoporous silica nanoparticle catalyst: excellent performance cyclohexane oxidation. *RSC Adv*. 2017;7:27506–27514. doi:10.1039/C7RA02280H

46. Melaiye A, Sun Z, Hindi K, et al. Silver(I)-imidazole cyclophane gem-diol complexes encapsulated by electro-spun tecophilic nanofibers: formation of nanosilver particles and antimicrobial activity. *JACS*. 2005;127:2285–2291. doi:10.1021/ja040226s

47. Kang S, Mauter MS, Elimelech M. Physicochemical determinants of multiwalled carbon nanotube bacterial cytotoxicity. *Environ Sci Technol*. 2008;42:7528–7534. doi:10.1021/es8010173

48. Shrifian-Esfahani A, Salehi MT, Nasr-Esfahani M, et al. Silver/Polyethylene oxide nanocomposite: UV-fabrication, characterization, and antibacterial activity. *Nanosci J*. 2012;12:4851.

49. In EUCAST disk diffusion method for antimicrobial susceptibility testing European society of clinical microbiology and infectious diseases Reading guide Version 3; 2013. s3

50. Sazegar MR, Jalil AA, Triwahyono S, et al. Protonation of Al-grafted mesostructured silica nanoparticles (MSN): acidity and catalytic activity for cumene conversion. *Chem Eng J*. 2014;240:352–361. doi:10.1016/j.cej.2013.12.004

51. Fernandes DM, Silva R, Winkler Heichenletner AA. Synthesis and characterization of ZnO, CuO and a mixed Zn and Cu oxide. *Mater Chem Phys*. 2009;115:110–115. doi:10.1016/j.matchemphys.2008.11.038

52. Liu J, Zhang L, Yang Q, et al. Structural control of mesoporous silicas with large nanopores in a mild buffer solution. *Microporous Mesoporous Mater*. 2008;116:330. doi:10.1016/j.micromeso.2008.04.030

53. Natarajan P, Khan HA, Yoon S, Jung KD. One-pot synthesis of Pt–Sn bimetallic mesoporous alumina catalysts with worm-like pore structure for n-butane dehydrogenation. *J Ind Eng Chem*. 2018;63:380–390. doi:10.1016/j.jiec.2018.02.038

54. Tian X, Zeng Y, Xiao T, Yang C, Wang Y, Zhang S. Fabrication and stabilization of nanocrystalline ordered mesoporous MgO–ZrO₂ solid solution. *Microporous Mesoporous Mater*. 2011;143:357–361. doi:10.1016/j.micromeso.2011.03.015

55. Trong D, Zaidi SMJ, Kaliaguine S. Stability of mesoporous aluminosilicate MCM-41 under vapor treatment, acidic and basic conditions. *Microporous Mesoporous Mater*. 1998;22:211–224. doi:10.1016/S1387-1811(98)00073-0

56. Mohamed NA, Fahmy MM. Synthesis and antimicrobial activity of some novel cross-linked chitosan hydrogels. *Int J Mol Sci*. 2012;13:11194–11209. doi:10.3390/ijms130911194

57. Triwahyono S, Abdullah Z, Jalil AA. The effect of sulfate ion on the isomerization of n-butane to iso-butane. *J Nat Gas Chem*. 2006;15:247–252. doi:10.1016/S1003-9953(07)60001-2

58. Alipour K, Nasirpour F. Smart anti-corrosion self-healing zinc metal-based molybdate functionalized-mesoporous-silica (MCM-41) nanocomposite coatings. *RSC Adv*. 2017;7:51879–51887. doi:10.1039/C7RA06923E

59. Tortora G, Funke RB, Case LC. *Microbiology—An Introduction*. New York: Longman; 2001.

60. Fernandes JC, Tavaria FK, Soares JC, et al. Antimicrobial effects of chitosans and chitooligosaccharides, upon Staphylococcus aureus and Escherichia coli, in food model systems. *Food Microbiol*. 2008;25:922. doi:10.1016/j.fm.2008.05.003

61. Balicka-Ramisz A, Wojtasz-Pajak B, Pilarczyk A, et al. Proceedings of 5th international conference on chitin and chitosan; Warsaw 2005: s406

62. Zhong ZY, Xiong ZT, Sun LF, et al. Nano-sized nickel (or cobalt)/graphite of composites for hydrogen storage. *J Phys Chem B*. 2002;106:9507–9513. doi:10.1021/jp020151j

63. Padmavathy N, Vijayaraghavan R. Enhanced bioactivity of ZnO nanoparticles—an antimicrobial study. *Sci Technol Adv Mater*. 2008;9:035004. doi:10.1088/1468-6996/9/3/035004

64. Shrifian-Esfahni A, Salehi MT, Nasr-Esfahni M, et al. Chitosan-modified superparamgnetic iron oxide nanoparticles: design, fabrication, characterization and antibacterial activity. *Chemik*. 2015;69 (1):19–32.

65. Hu M, Li C, Li X, et al. Zinc oxide/silver bimetallic nanoencapsulated in PVP/PCL nanofibres for improved antibacterial activity. *Artif Cells Nanomed Biotechnol*. 2017. doi:10.1080/216914012017136 6339

66. Kohanski MA, Dwyer DJ, Hayete B, et al. A common mechanism of cellular death induced by bactericidal antibiotics. *Cell*. 2007;130:797. doi:10.1016/j.cell.2007.06.049

67. Park HJ, Kim JK, Kim J. Silver-ion-mediated reactive oxygen species generation affecting bactericidal activity. *Water Res*. 2009;43:1027. doi:10.1016/j.watres.2008.12.002

68. Sunada K, Kikuchi Y, Hashimoto K, et al. Bactericidal and detoxification effects of TiO₂ thin film photocatalysts. *Environ Sci Technol*. 1998;32:726. doi:10.1021/es970860o

69. Fang M, Chen JH, Xu XL, et al. Antibacterial activities of inorganic agents on six bacteria associated with oral infections by two susceptibility tests. *Int J Antimicrob Agents*. 2006;27:513. doi:10.1016/j.ijantimicag.2006.01.008

70. Blake MD, Maness P, Huang Z, et al. Bactericidal activity of photocatalytic TiO₂ Reaction: toward an understanding of its killing mechanism. *Sep Purif Methods*. 1999;28:1. doi:10.1080/03602549 909351643

71. Stoimenov PK, Klinger RL, Marchin GL, et al. Metal oxide nanoparticles as bactericidal agents. *Langmuir*. 2002;18:6679. doi:10.1021/la0202374